

Simulation of viscous and inviscid rayleigh-taylor instability with surface tension by using MPS

Kyung Sung Kim^{1a} and Moo Hyun Kim^{*2}

¹*School of Naval Architecture and Ocean Engineering, Tongmyong University,
428 Sinseon-Ro, Nam-Gu, Busan, Republic of Korea*

²*Department of Ocean Engineering, Texas A&M University,
3136 TAMU, College Station, Texas, USA*

(Received February 5, 2018, Revised February 22, 2018, Accepted March 28, 2018)

Abstract. RTI (Rayleigh-Taylor instability) is investigated by a multi-liquid MPS (Moving Particle Semi-implicit) method for both viscous and inviscid flows for various density differences, initial-disturbance amplitudes, viscosities, and surface tensions. The MPS simulation can be continued up to the late stage of high nonlinearity with complicated patterns and its initial developments agree well with the linear theoretical results. According to the relevant linear theory, the difference between inviscid and viscous fluids is the rising velocity at which upward-mushroom-like RTI flow with vortex formation is generated. However, with the developed MPS program, significant differences in both growing patterns and developing speeds are observed. Also, more dispersion can be observed in the inviscid case. With larger Atwood (AT) number, stronger RTI flows are developed earlier, as expected, with higher potential-energy differences. With larger initial disturbances, quite different patterns of RTI-development are observed compared to the small-initial-disturbance case. If AT number is small, the surface tension tends to delay and suppress the RTI development when it is sufficiently large. Interestingly, at high AT number, the RTI-suppressions by increased surface tension become less effective.

Keywords: RTI (Rayleigh-Taylor instability); MPS (Moving Particle Semi-implicit) simulation; Atwood number; viscous vs. inviscid; initial disturbance; surface tension; RTI speed/pattern; mushroom-like RTI flows; comparison to linear theory

1. Introduction

Rayleigh-Taylor instability (RTI) is one of prominent phenomena for multi-phase flows. It occurs due to the gravitational instability of a heavy fluid overlying a lighter fluid. Examples include the behavior of water suspended above oil and mushroom clouds from atmospheric nuclear explosions. Under that condition, RTI tends to be generated with small initial perturbation. When lighter fluids move upward, the potential energy of the configuration becomes lower than the initial state. Thus the disturbance will grow and lead to a further release of potential energy. At the early stage, flow is generated from the small initial perturbations, which can be described by

*Corresponding author, Professor, E-mail: m-kim3@tamu.edu

^a Professor, E-mail: keiuskim@tu.ac.kr

the linearized equations, and then the instability grows exponentially. Later, with the rise of lighter fluid, the grown interface evolves to a mushroom-like curly form (called mushroom flows) and continues to further penetrate into the heavier fluid. The shape and size of initial perturbation is an important factor for the size and growth of RTI flows. However, the RTI is a mathematically ill-posed problem and the dependence on the initial condition is still an abstruse problem.

As aforementioned, at the early stage, the RTI can be described by linear equations when fluid is incompressible. The linear equations are based on a small-amplitude assumption and it predicts the exponential growth of the original disturbance (Taylor 1950). The results from the linear equations are shown to agree well with the relevant experiments in an early stage with small-amplitude perturbations (Chandrasekhar 2013, Waddell *et al.* 2001). However, the theory has limitations of predicting nonlinear phenomena associated with later-stage flows and large initial perturbations. The viscous effects are typical nonlinear term of Navier-Stokes' equation. According to (Sharp 1984), it was pointed out that numerical methods can often break down due to singularities on the interface. This singularities were investigated by (Moore 1979) by giving an asymptotic estimate of the critical time at the curvature along the interface which becomes infinite. (Cowley *et al.* 1999) further investigated the critical time by showing the singularities formed spontaneously in the complex plane at early times and then moved to intersect the real plane producing the curvature singularities.

(Krasny 1986) introduced a "vortex blob" method to make their numerical method compute beyond critical time of inviscid singularity formation. The idea is that the curvature singularity formed at the interface between inviscid fluids may trigger roll-up when the viscosity was considered. (Tryggvason *et al.* 1991) considered the effect of vortex-blob approach to the inviscid problem and then compared with viscous flow problem by solving Navier-Stokes' equation. (Tryggvason and Unverdi 1990) extended the numerical simulation into more complex geometry for RTI simulation.

As aforementioned, many numerical methods with fixed grid system may not compute RTI after the critical time. In this regard, the newly developed multi-liquid MPS is imposed to simulate RTI for much longer time. The MPS was originally introduced by (Koshizuka and Oka 1996) for the free-surface incompressible-fluid dynamics problems. It was subsequently developed by (Gotoh 2009) by improving the algorithm of particle interaction models. (Lee *et al.* 2011) adopted the new method of finding free-surface particle and further improved pressure-related algorithms. The MPS method has further been extended to multi-phase problems. (Khayyer and Gotoh 2013) solved high-density-ratio problem by introducing the interfacial averaged density. (Nomura *et al.* 2001) and (Shirakawa *et al.* 2001) introduced surface tension and buoyancy correction to better represent physics and improve accuracy under the condition of multi-liquids. The surface tension and buoyancy correction was further improved by (Kim *et al.* 2014). (Jeong *et al.* 2013) investigated the RTI by MPS method with corrective matrix for pressure calculation, which was proposed by (Khayyer and Gotoh 2011). With the improved multi-liquid algorithms, Kim and Kim (2017) investigated the Kelvin-Helmholtz instability phenomena at various interfaces. It needs to be mentioned that the very similar approach by SPH (smoothed particle hydrodynamics) can also handle the similar interfacial problems (e.g., Bakti *et al.* 2016), the details of which are not given in this introduction.

In this paper, a newly developed MPS method for multi-liquid systems with more robust algorithms including interface searching, self-buoyancy correction, and surface tension is applied to investigate the complex interfacial interactions and RTI instability phenomena. Various combinations of initial disturbance, surface tension, kinematic viscosity, and Atwood number

(density difference) were used to investigate the respective roles associated with the generation and development of RTI flows.

2. Moving Particle Semi-implicit (MPS) method

In order to simulate fluid dynamics numerically by Moving Particle Semi-implicit (MPS) Method, two equations which are continuity and Navier-Stokes equations are employed as governing equations. Two governing equations can be expressed as follows

$$\frac{D\rho}{Dt} = 0 \quad (1)$$

$$\frac{D\vec{u}}{Dt} = -\frac{1}{\rho}\nabla p + \nu\nabla^2\vec{u} + \sigma\kappa\vec{n} + \vec{F} \quad (2)$$

where ρ is density of fluid, t is time, \vec{u} is velocity of particle, p is pressure, ν is kinematic viscosity, σ is surface tension coefficient, κ is curvature of interface for surface tension, \vec{n} is normal vector of interface, \vec{F} is external force, ∇ denotes gradient, and ∇^2 represents Laplacian.

Since MPS is based on Lagrangian approach, all terms of differential operators should be replaced with the form of particle interaction method. The particle interaction method represents influence of neighboring particle to center particle, thus special treatment for considering effects from neighboring particle. In this regard, kernel function is employed to measure the effects of neighboring particles with respect to the distance from center particle to them. In this study, the following kernel function is employed

$$w(r_{ij}) = \begin{cases} \left(1 + \frac{r_{ij}}{r_e}\right)^3 \left(1 - \frac{r_{ij}}{r_e}\right)^3 & (0 < r_{ij} \leq r_e) \\ 0 & (r_e < r_{ij}) \end{cases} \quad (3)$$

where r_{ij} is distance between center and neighboring particle which can be calculated by $r_{ij} = r_j - r_i$, and r_e is critical range which can be regarded as effective range of center particle. In this study, default value of r_e is set to 2.1 by following (Lee *et al.* 2011).

Another special variance of MPS is particle number density. The MPS uses kernel function to keep the system to continuum, the density should be expressed by form of kernel function. In the entire MPS system, the particle number density act as density of fluid. The particle number density can be calculated by following formula.

$$n_i = \sum_{j \neq i} w(|\mathbf{r}_{ij}|) \quad (4)$$

Due to form of kernel function, the center particle is excluded from calculation unless it is necessary.

Aforementioned differential operators can be transferred by following particle interaction form and they can be expressed as follows

$$\langle \nabla \phi \rangle_i = \frac{d}{n_0} \sum_{j \neq i} \frac{\phi_{ij}}{|\mathbf{r}_{ij}|^2} \mathbf{r}_{ij} w(|\mathbf{r}_{ij}|) \quad (5)$$

$$\langle \nabla \cdot \phi \rangle_i = \frac{d}{n_0} \sum_{j \neq i} \frac{\phi_{ij} \mathbf{r}_{ij}}{|\mathbf{r}_{ij}|^2} w(|\mathbf{r}_{ij}|) \quad (6)$$

$$\langle \nabla^2 \phi \rangle_i = \frac{2d}{\lambda n_0} \sum_{j \neq i} [\phi_{ij} w(|\mathbf{r}_{ij}|)] \quad (7)$$

where

$$\lambda = \frac{\sum_{j \neq i} |\mathbf{r}_{ij}|^2 w(|\mathbf{r}_{ij}|)}{\sum_{j \neq i} w(|\mathbf{r}_{ij}|)} \quad (8)$$

Above equations Eqs. (5)-(7) represent gradient, divergence, and Laplacian operators written by particle interaction model, respectively. Moreover, n_0 denotes particle number density at the initial arrangement and λ is the parameter to make the increase of variance measured by distribution of particles equal to an increase of variance from unsteady diffusion equation.

In the MPS calculation routine, there is special algorithm to predict pressure on particle which is incompressibility model. It is similar to SMAC (Simplified Marker-and-Cell) method consisting two steps. The first step, explicit step, measures intermediate velocity of each particle, \vec{u}^* , due to viscosity, surface tension, and gravitational force.

$$\vec{u}^* = \left\{ \nu \nabla^2 \vec{u} + \sigma \kappa \vec{n} + \vec{g}z \right\} \Delta t \quad (9)$$

In this stage, the arrangement of particle can be moved with intermediate velocity, thus the satisfaction of the continuity equation can be violated. In this regard, concept of velocity corrector, \vec{u}' , which adjust particle arrangement in order to satisfy particle number density were introduced. The velocity corrector can be calculated by the pressure gradient and the pressure gradient was obtained by Poisson Pressure Equation (PPE) implicitly. (Lee *et al.* 2011) suggested multiple terms for poisson source to improve accuracy of prediction and to avoid nonphysical pressure fluctuation. The source term which is used in this study can be expressed as follow:

$$\nabla^2 p_i^{n+1} = \gamma \frac{\rho_0}{\Delta t^2} \frac{n_0 - n_i^n}{n_0} + (1 - \gamma) \frac{\rho_0}{\Delta t} \nabla \cdot \vec{u}^* \quad (10)$$

where superscriptions n or $n+1$ denote physical quantity at time n or $n+1$, γ is relaxation parameter which is less than 0.001. More detail information can be found in (Lee *et al.* 2011).

The fluid flow which has interface including free surface, the boundary condition is necessary

to satisfy boundary conditions. By tracing of particle, the kinematic boundary condition can be satisfied automatically. The dynamic boundary condition can be satisfied by taking reference pressure on the interface particles. For free surface particle, the reference pressure should be atmosphere pressure and the interface between fluid-fluid layers can be summation of interface particle with different phase within effective range.

To apply the dynamic boundary condition, indication of interface particle should be established first. At the interface region, the particle number density with same fluid phase decreases since there is no particle for free surface or there are different types of particles. In this regard, the following simple conditions are employed to identify the interface particles

$$\beta_1 n_0 < n_i < \beta_2 n_0 \tag{11}$$

$$N_i < \beta_3 N_0 \tag{12}$$

where β_1, β_2 , and β_3 are parameters below 1.0, N_i is number of particle within effective range for center particle I, and N_0 is maximum number of particle at the initial arrangement. In this formula, only particle with same type are involved. More detail information can be found in (Kim *et al.* 2014). In this study, β_1, β_2 , and β_3 set to 0.3, 0.97, and 0.85, respectively. By using boundary condition with interface particle tracing method can make MPS to simulate fragmentation and coalescence of interface including free surface.

A repulsive force can be generated by local pressure, however, it may be improperly calculated when particles get close too much, especially large deformation due to coalescence or fragmentation of free surface and interface. As a result of large deformation, the particle number density may have sudden increase, which leads spatial instability of the pressure. Therefore, collision model was employed to stabilize the pressure field.

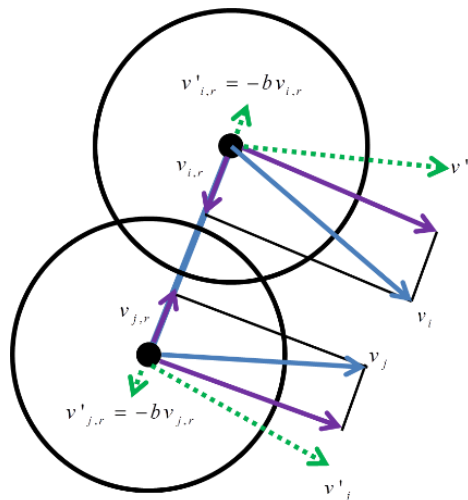


Fig. 1 Schematic of Collision Model

The schematic of collision model is shown in Fig. 1. When the distance between any two particles gets smaller than criterion, the collision model is applied. The criterion is al_0 , where l_0 is particle distance at initial arrangement, and a is arbitrary number. The repulsive velocity can be calculated by using repulsive coefficient, b , which is defined as the ratio of normal velocity to opposing particle, $b = -v'_r/v_r$, where the subscript r denotes the velocity normal to the opposing particle. The parameters, a and b are set to 0.85 and 0.2 recommended by (Lee *et al.* 2011).

Since particle method is following Lagrangian approach, it is easy to identify interface particle with indication method, however, in the view point of surface tension, the variance which is curvature cannot be measured due to complexation of drawing the interface layer. In this regard, two additional particle number density were adopted

$$\begin{aligned} n_i^{st1} &= \sum_{j \neq i} w^{st1}(|r_{ij}|) \\ n_i^{st2} &= \sum_{j \neq i} w^{st2}(|r_{ij}|) \end{aligned} \quad (13)$$

Where

$$\begin{aligned} w^{st1} &= \begin{cases} 1 & (0 < r \leq r_e^{st}) \\ 0 & (r > r_e^{st}) \end{cases} \\ w^{st2} &= \begin{cases} 1 & (0 < r \leq r_e^{st} \text{ and } n_j^{st1} > n_i^{st1}) \\ 0 & (\text{otherwise}) \end{cases} \end{aligned} \quad (14)$$

Where r_e^{st} is effective range for surface tension and it is set to 3.1 in this study. With newly adopted kernel function, the curvature for surface tension can be calculated by following formula:

$$\kappa = \frac{1}{R} = \frac{2}{r_e^{st}} \cos\left(0.5\pi \frac{n_i^{st2}}{n_0^{st1}}\right) \quad (15)$$

Another unknown variance for surface tension is normal vector and it can be estimated by following formula

$$\vec{a}_i = \sum x_n \mathbf{n}_x + \sum y_n \mathbf{n}_y \quad \text{and} \quad \vec{n}_i = \frac{\vec{a}_i}{|\vec{a}_i|} \quad (16)$$

Involved particle in interface particles are same physical properties only. More detail information regarding to surface tension can be found in (Kim *et al.* 2014).

3. Simulation results and discussions

3.1 Previous validation of the multi-liquid MPS program

The developed MPS program for a single fluid has been verified by various CFD results and experimental results of a typical water-flow-by-broken-dam case (Bakti *et al.* 2016). It was also extensively verified for liquid sloshing against many experimental results (Kim and Kim 2014, Bakti *et al.* 2016). The multi-liquid-sloshing cases with multiple interfaces including interfacial Kelvin-Helmholtz instability have been verified against Molin's experimental results in Kim and Kim (2014, 2017) and Kim *et al.* (2015).

3.2 RTI simulation examples: Vertical pipe with multi-liquids

Next, let us consider the simulation of RTI by using newly developed MPS method and the schematic model is shown in Fig. 2. In the vertical pipe, two different fluids were located and in order to obtain spontaneous gravitational acceleration and heavier fluid was located over lighter fluid. For the repeatability, the initial perturbation exists at the interface between two fluids. The fluid is placid at the beginning, and then it starts to flow by an imposing destabilizing acceleration as time increases. In this situation, the pressure and density gradients are in opposite direction. In this simulation, 22,500 particles were used for lighter fluid, and same number was used for heavier fluid. The wall and dummy particle consumed 6,100 particles.

3.3 Effect of Atwood number

The selected simulation model for RTI has two fluids in vertical pipe and the heavier fluid is located over lighter fluid, so the rising flow can be generated spontaneously. In this regard, the density difference between two fluids are most important factor to generate momentum for subsequent flow. In this section, several sets of density differences are applied to observe the density-difference effects. The density difference can be expressed by Atwood number(AT), which is the ratio of densities as follows

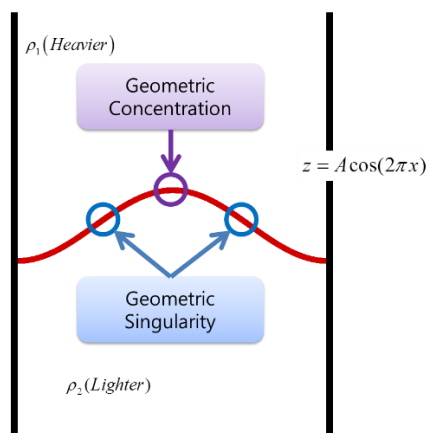


Fig. 2 Numerical Model for RTI

$$AT = \frac{|\rho_1 - \rho_2|}{\rho_1 + \rho_2} \quad (17)$$

Aforementioned, in this case, the density difference and gravity/buoyancy force is the main cause of RTI. To investigate the effects of RTI on density differences, various Atwood numbers are considered. The selected Atwood numbers were 0.2, 0.4, and 0.6 and the surface tension coefficient was set to 0.023 N/m . Fig. 3 shows the snapshots obtained from the simulation results at various times. In this simulation, the kinematic viscosity was fixed to $1.0 \times 10^{-2} \text{ m}^2/\text{s}$. At much lower kinematic viscosity than that, it may have problems to simulate RTI (Forbes 2009). The simulation was started from the initial free-surface shape of $A \cos(kx)$ where A is amplitude of disturbance.

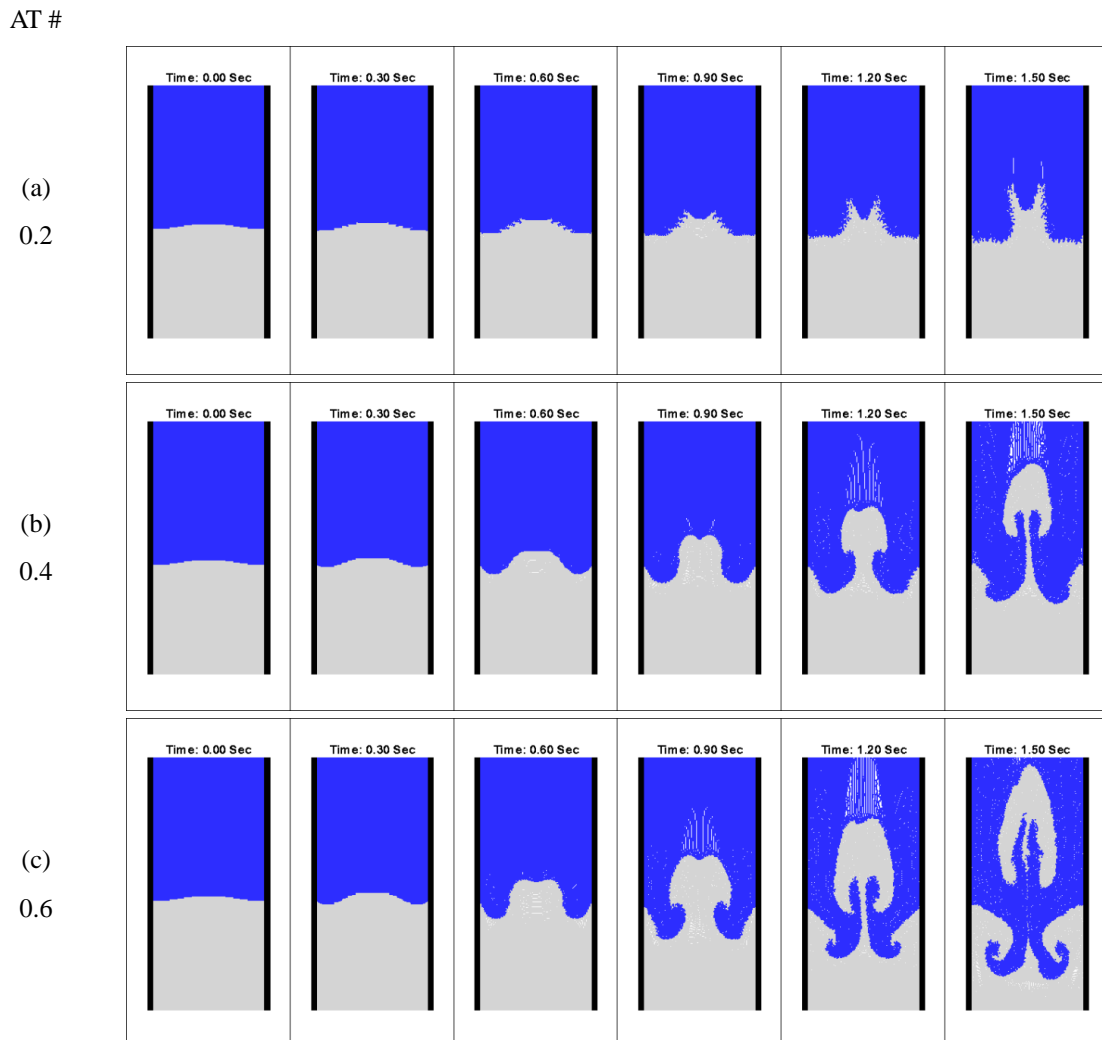


Fig. 3 Evolution of Flow Development with various AT numbers

The first row of Fig. 3 [Fig. 3(a)] shows the time marching interface shapes for the lowest Atwood number. The split-peak rising flows were observed. However, Atwood #=0.4 and 0.6 cases show the mushroom-like overturning flows, which is the typical pattern of RTI. At the highest AT #, the mushroom head becomes larger, rises faster, and is detached earlier from the main body. In general, the overturning flow called wake can be induced by the diffusion term of Navier-Stoke's equation. The reason of not showing RTI at WT=0.2 is due to insufficient initial energy at the given initial profile. Another interesting point in this simulation is the breaking of interface was triggered at the singularities in the case of lowest AT while the breaking started at the concentration for other cases. Through the comparison of Atwood number of system, it is revealed that the density difference is prominent component to trigger RTI flows.

Amplitude

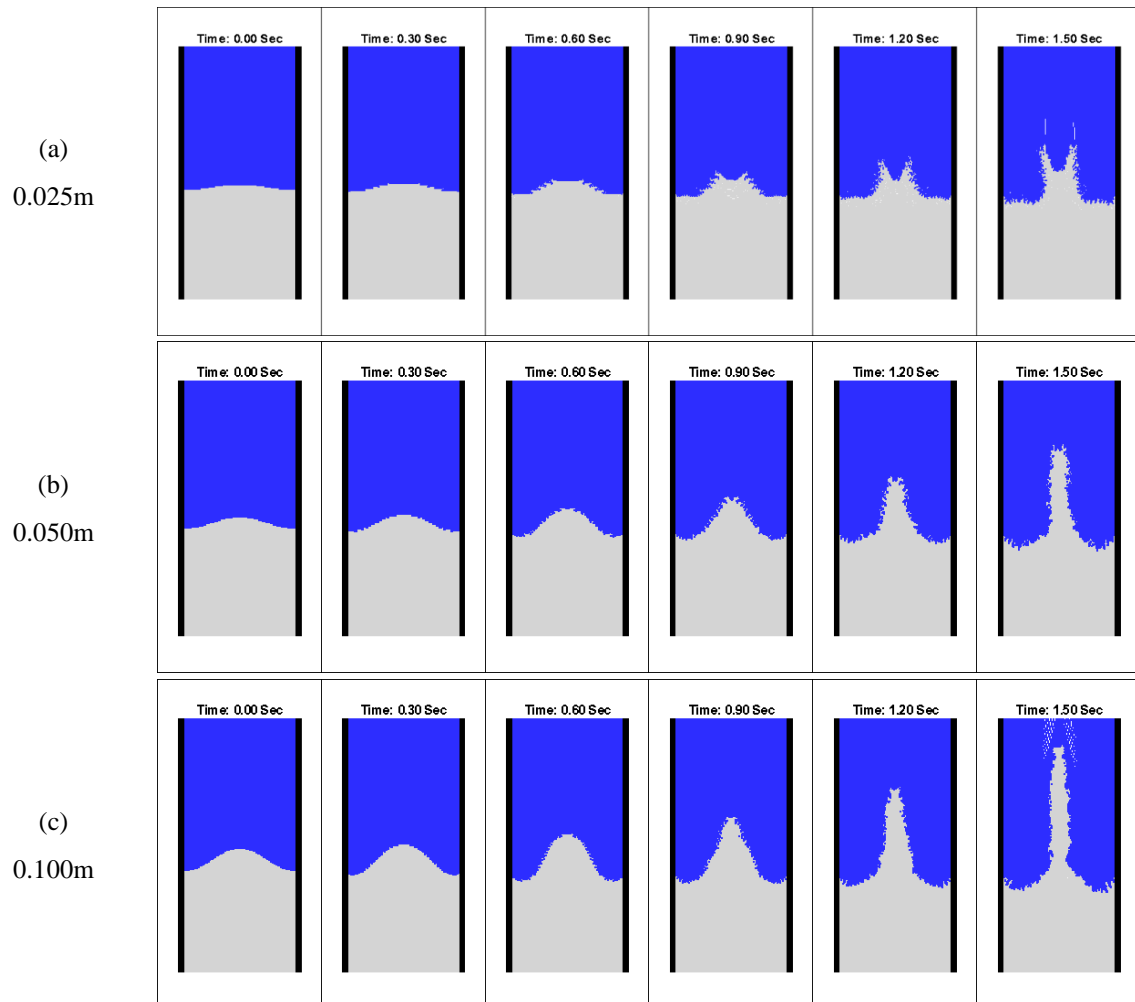


Fig. 4 Evolution of Flow Development with various initial-disturbance amplitudes

3.4 Effects of the amplitude of initial disturbance

In the previous section, it is shown that the density difference between fluids is a significant factor to generate RTI flow. In the case of the low Atwood number=0.2, the rising flow with split peaks were developed without mushroom-like overturning. For this case, the effects of initial-disturbance amplitudes are observed in Fig. 4. The range of initial amplitudes was set to 0.025 m to 0.1 m. The other simulation conditions were exactly same as those of Fig. 3. When the initial amplitude is 0.025 m, rising flows were developed at the two singular points. On the contrary, with initial disturbance higher than 0.05 m, one column of rising flow is developed at the center position. The rising velocity increases with initial disturbance. In all cases, the mushroom-like RTI flow is not observed since the density difference is not large enough. In summary, with the increase of initial-disturbance amplitudes, the typical symmetric-tooth-like split-peak patters, which can be predicted by the linear theory, are not generated. Instead, one prominent center jet is generated.

3.5 Effects of viscosity

Another prominent factor for RTI is viscosity. According to the Navier-Stoks' equation, Eq. (2), the viscous effects can be measured by the diffusion term with Laplacian operator. In Fig.5, the same simulations as Fig. 3 was performed with inviscid-fluid condition i.e., the kinematic viscosity is set to zero. According to the investigation by Sharp (1984), the numerical methods with fixed-grid system broke down for this kind of case since the fixed-grid method may failed to calculate singularities. However, the present particle based Lagrangian approach does not have that kind of restriction and it is able to simulate inviscid flow RTI beyond the critical point. Similar behaviors may be observed in the cases with very low viscosity.

The sequence of snap-shots of Fig. 5 coincides with that of Fig. 3, high viscosity vs. no-viscosity. Interestingly at WT=0.2 and A=0.025 m, the initial development pattern is similar between Figs. 3(a) and 5(a) but at later stage, the inviscid case shows RTI with horizontal mushrooms at both sides since the instability and curly flows are not limited by viscosity. With increased AT numbers in Figs. 5(b) and 5(c), similar patterns as Fig. 5(a) are developed with increased speed and in more widely spread patterns, which eventually leads to a very wide turbulence mixture region without clear pattern. The overall pattern with two horizontal mushrooms is quite different from the single vertical mushroom shape with viscosity. From the comparison, we can conclude that the viscosity is an important factor for the development and pattern of RTI.

Baker *et al.* (1993) presented a formula to estimate critical time for calculation break down as follows

$$t_c = \sqrt{\frac{1}{At}} \log\left(\frac{1}{A}\right) \quad (18)$$

where t_c denotes critical time of calculation, and A denotes amplitude of initial perturbation. In the simulation of AT=0.2 and A=0.025 m, the critical time equals to 3.58 sec. In this regard, Fig. 6 represents snapshots after 2.0 sec in the cases of inviscid and viscous fluids with Atwood number=0.2. From the comparison of snapshots, it is seen that after the critical time, the form of flows was clearly distinguished. In the case of no-viscosity, the lighter fluid flew to lateral

direction to form mushroom shape. In this case, the low buoyancy force could not penetrate the heavier upper fluid and then the residue of energy developed the lateral flow. Eventually, the RTI flow was dissipated by convection. In contrast, the viscous fluid continuously flows upward, and then it turned into the RTI flows when the system has the energy to produce over-turning flows. Through this comparison, it is revealed that both inviscid and viscous fluids can generate typical RTI flows when the system met the conditions. However, due to the viscous effects, the initiation of RTI is delayed.

In linear theory, the perturbation can grow exponentially and the maximum interfacial displacement can be measured by the following equation.

$$\eta(t) = A \exp(\omega t) \tag{19}$$

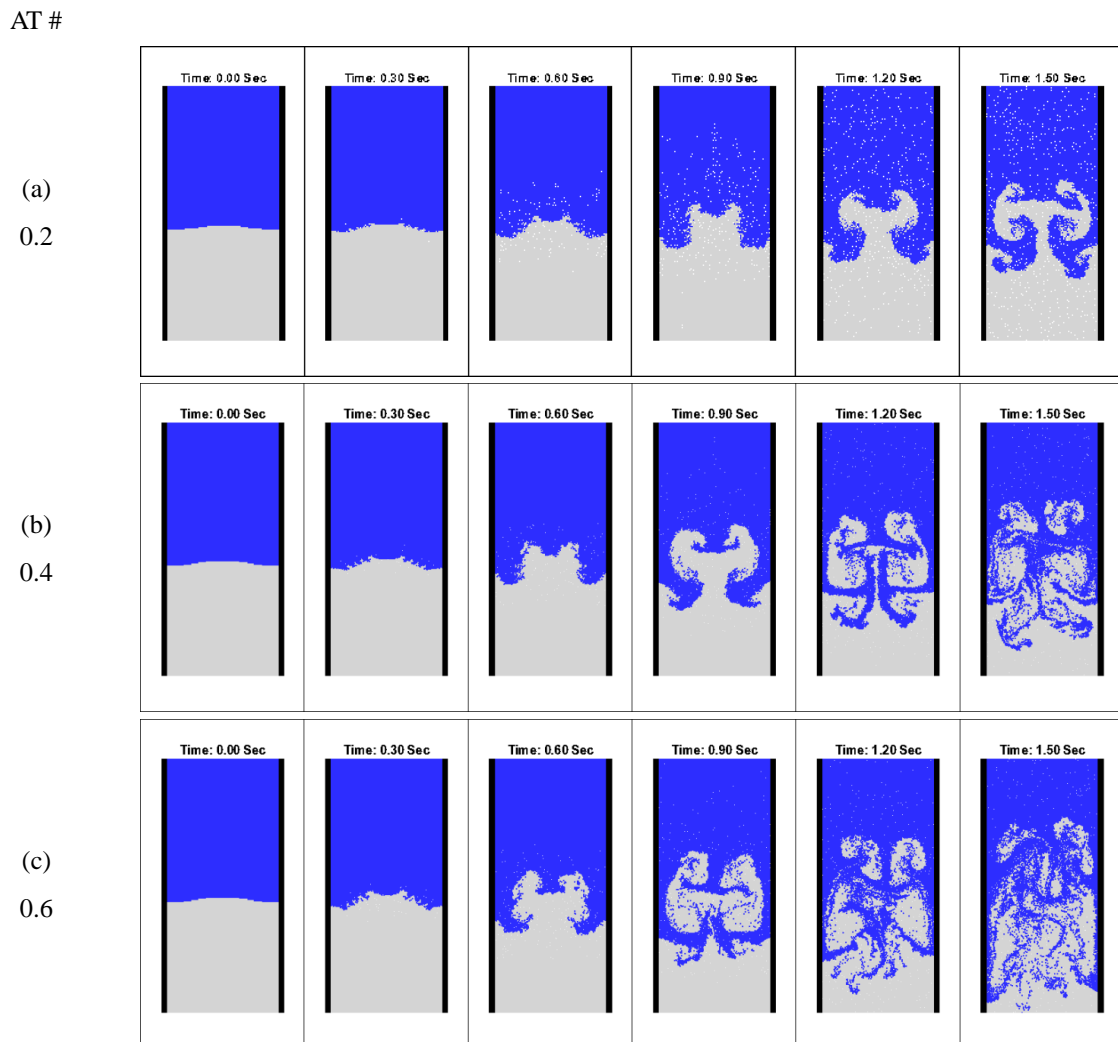


Fig. 5 Evolution of Flow Development for Inviscid Fluid

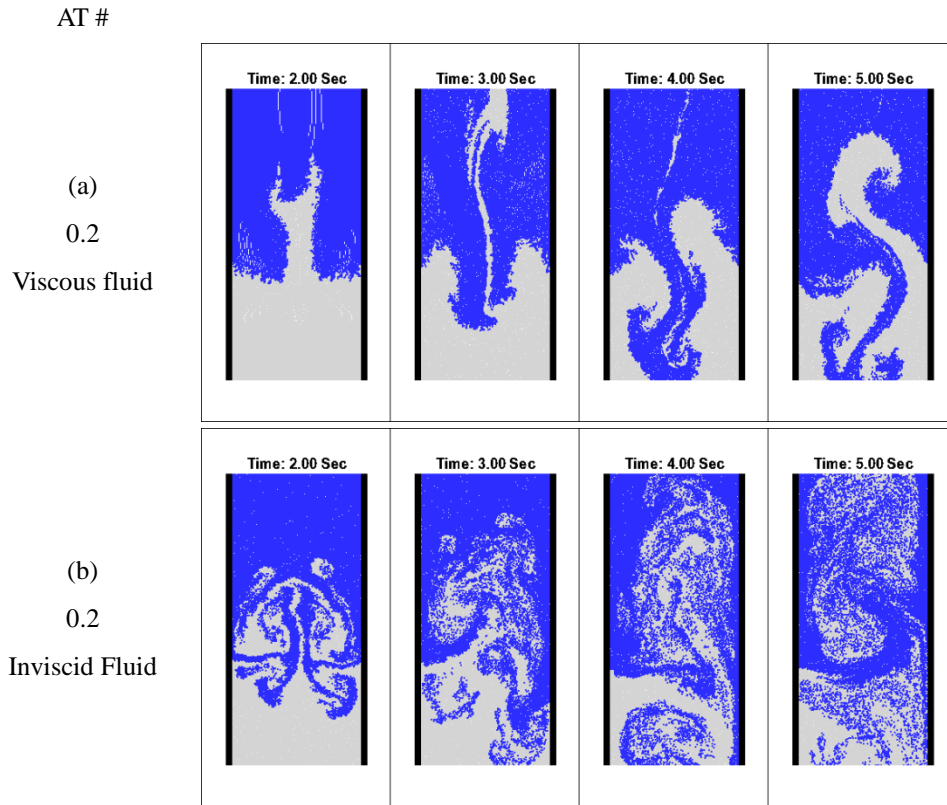


Fig. 6 Evolution of Flow Development for Viscous and Inviscid Fluid after the Critical Time

where η is displacement of interface, ω is growth rate, A is amplitude of initial disturbance, and t is time. By taking positive roots, the growth rate of RTI for viscous fluid can be expressed as follows (Mikaelian 1996)

$$\omega^2 + 2\nu k^2 \omega - ATgk \left(1 - \frac{k^2}{k_c^2} \right) = 0 \quad (20)$$

where k is wave number, k_c is reference wave number, ν is kinematic viscosity, and AT is Atwood number. The reference wave number can be calculated by the following formula

$$k_c = \sqrt{\frac{(\rho_2 - \rho_1)g}{T}} \quad \text{where } T \text{ is surface tension} \quad (21)$$

Since the scaled velocity and characteristic time are defined by $\sqrt{\lambda g}$ and $\sqrt{\lambda/g}$, the relevant dimensionless parameters, dimensionless time (τ_{RT}^*) and interface displacement (η_{RT}^*), can be expressed as follows

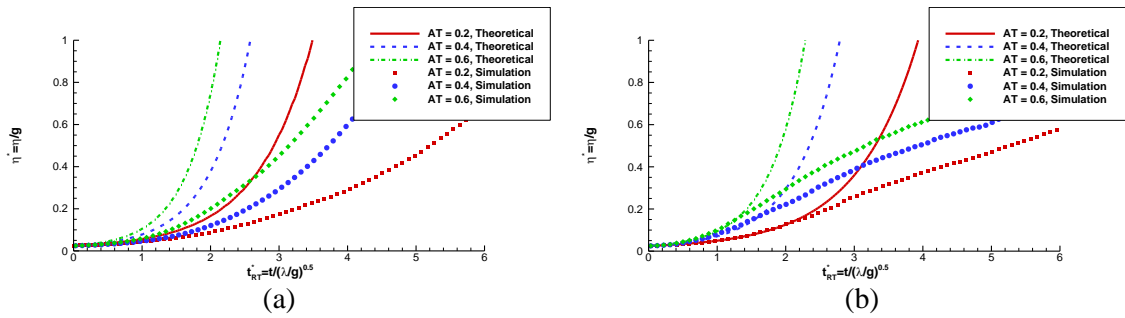


Fig. 7 Comparison of growth rate between theoretical and numerical values for (a) viscous fluid and (b) inviscid fluid

Properties

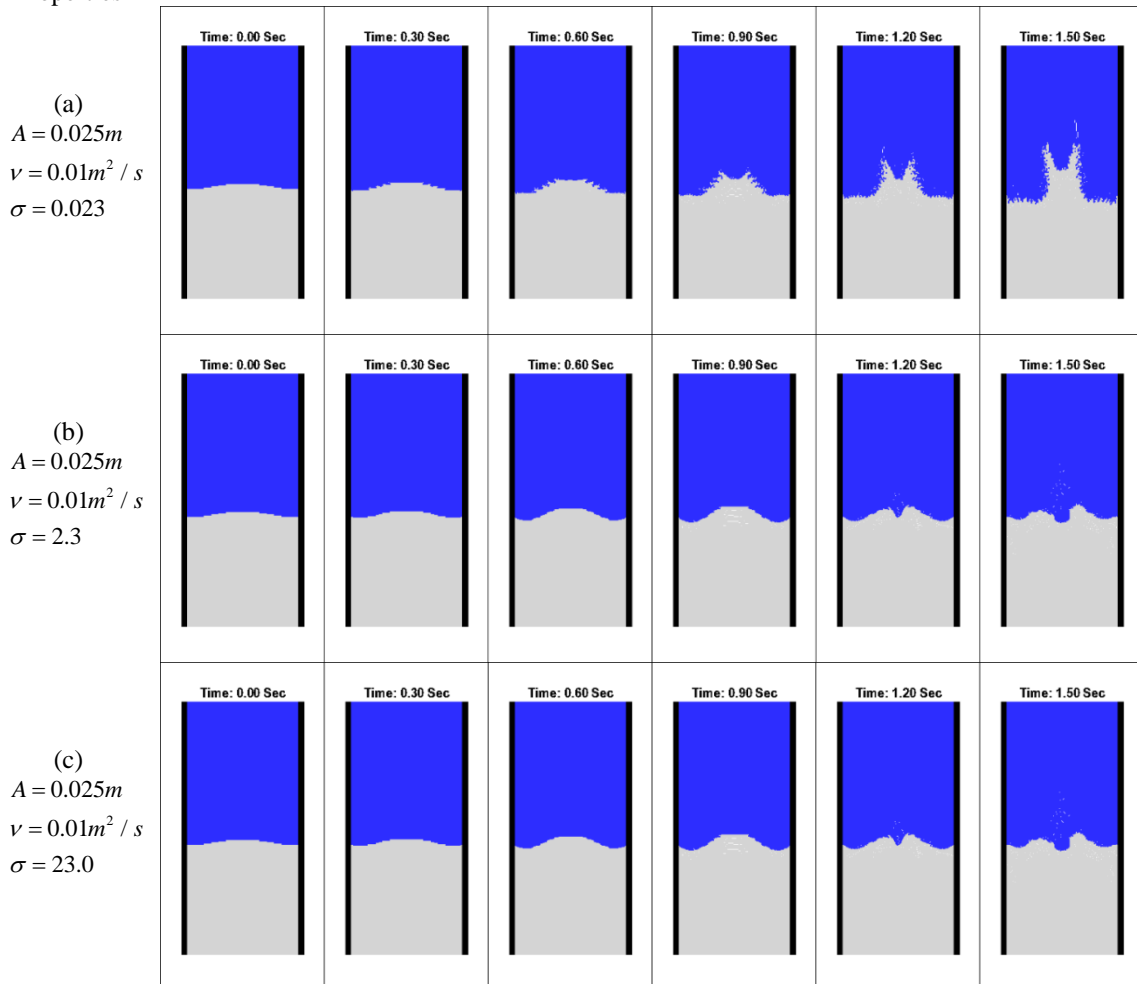


Fig. 8 Evolution of Flow Development for Viscous Fluid with various surface with tension coefficients (AT=0.2)

Properties

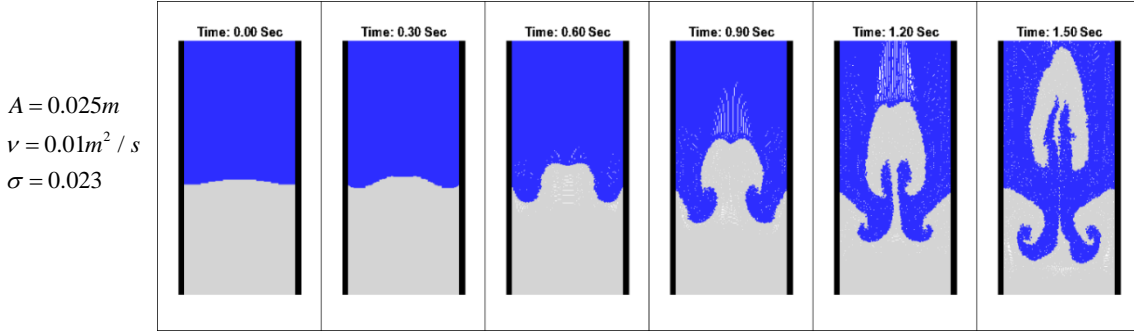


Fig. 9 Evolution of flow development for viscous fluid with surface tension coefficient=2.3 and AT=0.6

$$\tau_{RT}^* = t \sqrt{\frac{g}{\lambda}} \quad (22)$$

$$\eta_{RT}^* = \frac{\eta}{\lambda} \quad (23)$$

By solving Eq. (20), the interface displacement can be measured and then the non-dimensional interface evolution can be calculated by using Eq. (22). According to the theory, the interface disturbance grows exponentially both in inviscid and viscous fluids. Those theoretical interface evolutions for viscous and inviscid fluids were compared with those of numerical simulations in Figs. 7(a) and 7(b). For viscous fluid, both theoretical and numerical results show exponential growth of interface with time although the growth rates can be different after some time. On the other hand, the results of inviscid fluids show different trend between theoretical and numerical solutions despite better initial agreement up to the extended period of time compared to Fig. 7(a). The theory is based on the linear theory and is to be valid only during the initial growth period of RTI before reaching highly nonlinear stage.

3.6 Effects of surface tension

In this section, the effects of surface tension on RTI are discussed. In the previous simulations, the surface tension coefficient was set as 0.023. Usually, the surface tension at the interface between water and air is 0.076. However, as hypothetical fluids, the surface tension was varied from 0.023 to 2.3 and 23 in Fig. 8 while fixing AT=0.2 and kinematic viscosity=0.01.

Fig. 8 shows the progressive snapshots with time from each case. As shown in this comparison, the rising flow with two split peaks can be observed when surface tension=0.023. When the surface tension is increased to 2.3, the development of rising flows with dual sharp peaks is suppressed by much stronger surface tension and we can only observe dual rounded small disturbances at the interface. If we further increase the surface tension to 23, there is little difference compared to ST=2.3 case, which means that after the interface is sufficiently suppressed

and rounded, the surface-tension effects only play minor role for the interfacial disturbances. On the other hands, when Atwood number is high (e.g., 0.6), the momentum for RTI flow is large enough to overcome the surface tension force as shown in Fig. 9.

4. Conclusions

The Rayleigh-Taylor instability at the interface of two fluids of different densities is investigated with varying densities, initial disturbances, viscosities, and surface tensions by using the newly developed MPS method for multi-phase fluids. The classical RTI example for two different fluids interfaced in vertical pipe was examined. To generate destabilizing acceleration, the heavier fluid is located over the lighter fluid. Moreover, initial perturbations were applied at their interface to stimulate the subsequent flow development.

With various Atwood numbers, it was seen that the typical RTI pattern, which is mushroom shape flow, was observed except the case of the lowest Atwood number. The development of RTI is also delayed with smaller initial disturbances and density differences. The density difference is prominent component to generate RTI flows and their strength. When the fluid is inviscid, the typical RTI pattern is developed earlier than the case with viscosity but the boundary of interface becomes less clear due to more dispersion. Therefore, the viscosity is related to the strength of diffusion/dispersion and energy dissipation. In the general CFD method with fixed grid system, the calculation is broken down by the restriction of mesh structure. However, the present particle method can continue even after the critical time. As a result, the simulations for both inviscid and viscous fluids can be continued.

Another investigation performed in this study was the effects of surface tension on the RTI. When AT is low, the surface tension tends to delay and suppress the development of RTI depending on its magnitude. However, after the interface was sufficiently rounded, its effects became less important. When AT is large enough to generate strong RTI flow, the surface tension effects play little role since it is hard to prevent the strong momentum of the penetration flow.

The example RTI simulations for various cases demonstrated the role of density difference, initial disturbance, viscosity, and surface tension. The present two-fluid MPS can robustly continue the RTI flows even after later stage with high nonlinearity compared to the early breakdown of simulation by conventional grid-based CFD methods.

Acknowledgements

This research was supported by Basic Science Research Program through the National Research Foundation of Korea(NRF) funded by the Ministry of Education(NRF-2018R1D1A1B07048254) and Tongmyong University Research Grants 2018(2018F026)

References

Baker, G., et al. (1993), "Singularity formation during Rayleigh–Taylor instability", *J. Fluid Mech.*, **252**, 51-78.

- Bakti, F.P., Kim, M.H., Kim, K.S. and Park, J.C. (2016), "Comparative study of standard WC-SPH and MPS solvers for free-surface academic problems", *J. Offshore Polar.*, **26**(3), 235-243.
- Chandrasekhar, S. (2013), Hydrodynamic and hydromagnetic stability, Courier Corporation.
- Cowley, S.J., et al. (1999), "On the formation of Moore curvature singularities in vortex sheets", *J. Fluid Mech.*, **378**, 233-267.
- Gotoh, H. (2009), Lagrangian Particle Method-Advanced Technology for Numerical Wave Flume. The Nineteenth International Offshore and Polar Engineering Conference, International Society of Offshore and Polar Engineers.
- Jeong, S.M., et al. (2013), "Numerical prediction of oil amount leaked from a damaged tank using two-dimensional moving particle simulation method", *Ocean Eng.*, **69**, 70-78.
- Khayyer, A. and Gotoh, H. (2011), "Enhancement of stability and accuracy of the moving particle semi-implicit method", *J. Comput. Phys.*, **230**(8), 3093-3118.
- Khayyer, A. and Gotoh, H. (2013), "Enhancement of performance and stability of MPS mesh-free particle method for multiphase flows characterized by high density ratios", *J. Comput. Phys.*, **242**, 211-233.
- Kim, K.S., et al. (2014), "Development of moving particle simulation method for multiliquid-layer sloshing", *Math. Probl. Eng.*
- Kim, K.S. and Kim, M.H. (2017), "Simulation of Kelvin Helmholtz instability by using MPS method" *Ocean Eng.*, **130**, 531-541.
- Kim, K.S. and Kim, M.H. and Park, J.C. (2015), "Simulation of multi-liquid-layer sloshing with vessel motion by using moving particle simulations", *J. Offshore Mech. Arct.*, **137**(5),
- Koshizuka, S. and Oka, Y. (1996), "Moving-particle semi-implicit method for fragmentation of incompressible fluid", *Nuclear Sci. Eng.*, **123**(3), 421-434.
- Krasny, R. (1986), "Desingularization of periodic vortex sheet roll-up", *J. Comput. Phys.*, **65**(2), 292-313.
- Lee, B.H., et al. (2011), "Step-by-step improvement of MPS method in simulating violent free-surface motions and impact-loads", *Comput. Method. Appl. M.*, **200**(9), 1113-1125.
- Mikaelian, K.O. (1996), "Rayleigh-Taylor instability in finite-thickness fluids with viscosity and surface tension", *Phys. Rev.*, **54**(4), 3676.
- Moore, D. (1979), "The spontaneous appearance of a singularity in the shape of an evolving vortex sheet", *Proceedings of the Royal Society of London A: Mathematical, Physical and Engineering Sciences*, The Royal Society.
- Nomura, K., et al. (2001), "Numerical analysis of droplet breakup behavior using particle method", *J. Nuclear Sci. Technol.*, **38**(12), 1057-1064.
- Sharp, D.H. (1984), "An overview of Rayleigh-Taylor instability", *Physica D: Nonlinear Phenomena*, **12**(1), 3-18.
- Shirakawa, N., et al. (2001), "Analysis of the void distribution in a circular tube with the two-fluid particle interaction method", *J. Nuclear Sci. Technol.*, **38**(6), 392-402.
- Taylor, G. (1950), "The instability of liquid surfaces when accelerated in a direction perpendicular to their planes. I", *Proceedings of the Royal Society of London A: Mathematical, Physical and Engineering Sciences*, The Royal Society.
- Tryggvason, G., et al. (1991), "Fine structure of vortex sheet rollup by viscous and inviscid simulation", *J. Fluid Eng.*, **113**(1), 31-36.
- Tryggvason, G. and Unverdi, S.O. (1990), "Computations of three-dimensional Rayleigh-Taylor instability", *Phys. Fluids A: Fluid Dynam.*, (1989-1993) **2**(5), 656-659.
- Waddell, J., et al. (2001), "Experimental study of Rayleigh-Taylor instability: low Atwood number liquid systems with single-mode initial perturbations", *Phys. Fluids.*, (1994-present) **13**(5), 1263-1273
- Forbes, L.K. (2009), "The Rayleigh-Taylor Instability for inviscid and viscous fluids", *J. Eng. Math.*, **65**(3), 273-290